Title
Hydroxyl Radical Production by Air Pollutants in Epithelial Lining Fluid Governed by Interconversion and Scavenging of Reactive Oxygen Species

Journal
Environmental Science and Technology, 55(20)

ISSN
0013-936X

Authors
Lelieveld, Steven
Wilson, Jake
Dovrou, Eleni
et al.

Publication Date
2021-10-19

DOI
10.1021/acs.est.1c03875

Peer reviewed

Environmental Science & Technology

pubs.acs.org/est

Article

Hydroxyl Radical Production by Air Pollutants in Epithelial Lining Fluid Governed by Interconversion and Scavenging of Reactive Oxygen Species

Steven Lelieveld, Jake Wilson, Eleni Dovrou, Ashmi Mishra, Pascale S. J. Lakey, Manabu Shiraiwa, Ulrich Pöschl, and Thomas Berkemeier*

Cite This: *Environ. Sci. Technol.* 2021, 55, 14069−14079

Read Online

ACCESS | Metrics & More | Article Recommendations | Supporting Information

ABSTRACT: Air pollution is a major risk factor for human health. Chemical reactions in the epithelial lining fluid (ELF) of the human respiratory tract result in the formation of reactive oxygen species (ROS), which can lead to oxidative stress and adverse health effects. We use kinetic modeling to quantify the effects of fine particulate matter (PM2.5), ozone (O_3), and nitrogen dioxide (NO_2) on ROS formation, interconversion, and reactivity, and discuss different chemical metrics for oxidative stress, such as cumulative production of ROS and hydrogen peroxide (H_2O_2) to hydroxyl radical (OH) conversion. All three air pollutants produce ROS that accumulate in the ELF as H_2O_2, which serves as reservoir for radical species. At low PM2.5 concentrations (<10 μg m^{-3}), we find that less than 4% of all produced H_2O_2 is converted into highly reactive OH, while the rest is intercepted by antioxidants and enzymes that serve as ROS buffering agents. At elevated PM2.5 concentrations (>10 μg m^{-3}), however, Fenton chemistry overwhelms the ROS buffering effect and leads to a tipping point in H_2O_2 fate, causing a strong nonlinear increase in OH production. This shift in ROS chemistry and the enhanced OH production provide a tentative mechanistic explanation for how the inhalation of PM2.5 induces oxidative stress and adverse health effects.

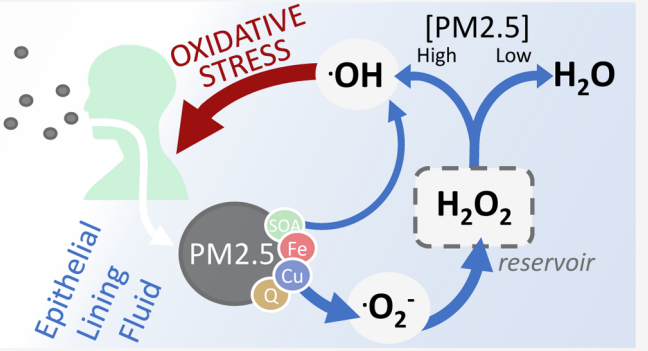

KEYWORDS: *reactive oxygen species, PM2.5, epithelial lining fluid, oxidative stress*

INTRODUCTION

Ambient air pollution is responsible for 4−9 million excess deaths per year.[1−3] Air pollutants can cause and exacerbate ischemic heart disease (e.g., myocardial infarction), cerebrovascular disease (e.g., stroke), lower respiratory infections (e.g., pneumonia), and chronic obstructive pulmonary disease (COPD).[4−6] The air pollutants that most strongly correlate with negative health outcomes are nitrogen dioxide (NO_2), ozone (O_3), and fine particulate matter with a diameter less than 2.5 μm (PM2.5), with the latter likely contributing more than 80% to the total excess mortality.[7,8]

PM2.5 is a complex mixture that can encompass thousands of different chemical constituents, each having distinct properties. PM2.5 originates from both natural and anthropogenic sources, including mineral dust from deserts, gasoline and diesel motor exhausts, tire and brake wear, power generation, residential energy use, agriculture, biomass burning, cooking, and cigarette smoking. Because of the great heterogeneity in both PM2.5 composition and sources, targeted PM2.5 pollution control is challenging, and, to date, there is no clear connection between one particular PM2.5 constituent and mortality estimates.[9−12] In spite of fundamental challenges studying causal relationships between air pollutants and health outcomes, it has been generally accepted that the underlying pathology of air pollutant exposure includes oxidative stress and systemic inflammation.[7,13−15] Moreover, in recent years, the oxidative potential of PM2.5 has become a common metric for measuring PM2.5 toxicity.[13,16−19] The oxidative potential of PM2.5 has been shown to vary greatly among sampling sites and proximity to the emitting source.[16,20−22] Based on case-crossover studies, it has been suggested that the risk of respiratory illness and myocardial infarction was increased in exposure episodes with high PM2.5 oxidative potential.[13,23]

PM2.5 contains redox-active components, most notably copper, iron, secondary organic aerosols (SOA), and quinones, which trigger the formation of reactive oxygen species (ROS)

Received: June 12, 2021
Revised: September 6, 2021
Accepted: September 17, 2021
Published: October 5, 2021

https://doi.org/10.1021/acs.est.1c03875
Environ. Sci. Technol. 2021, 55, 14069−14079

in the epithelial lining fluid (ELF) of the respiratory tract.[14,24−28] The umbrella term "ROS" encompasses several highly reactive molecules, including hydrogen peroxide (H_2O_2), the hydroperoxyl radical (HO_2), the superoxide radical anion (O_2^-), and the hydroxyl radical (OH).[29] Their reactivity and stability vary greatly, with H_2O_2 being the most stable, and OH the most reactive.[30] ROS may induce oxidative stress and inflammation in the ELF, thereby causing adverse health effects.[14,24,31−33]

NO_2 is an irritant gas that has been linked to mortality in epidemiological studies.[34,35] However, because NO_2 is often co-emitted with PM2.5 and other pollutants in combustion processes, it remains unclear if it poses an independent health risk.[36,37] In the ELF, NO_2 can consume antioxidants and form nitrite (NO_2^-) in the process.[38,39] The oxidized forms of antioxidants are typically nontoxic, but their reactive intermediates have been suggested to form ROS in small yields in the case of the glutathiyl radical.[39,40]

Exposure to O_3 has been shown to exacerbate asthma and increase respiratory and circulatory mortality.[8,41,42] It is known to react with alkenes by addition to the C−C double bond, leading to lipid peroxidation and forming a variety of oxidized reaction products, including Criegee intermediates and hydroperoxides.[43−45] However, while the chemical properties of NO_2 and O_3 are well understood, the mechanisms behind their health effects and contribution to ROS formation in the ELF, remain unclear.

In cells, several mechanisms prevent the formation of ROS, or intercept these highly reactive molecules before causing oxidative stress.[30] The interception of ROS includes chemical reactions leading to unreactive products (ROS scavenging) and chemical conversion into less reactive ROS.[30,46] In the ELF, this task is fulfilled by low-molecular-mass antioxidants and antioxidant enzymes.[14,24,47] The enzyme superoxide dismutase (SOD) efficiently shuttles O_2^- into the less reactive H_2O_2, whereas the enzyme catalase is the major natural sink of H_2O_2 in the ELF.[48] Together, these endogenous processes lead to a ROS buffering effect that helps to maintain physiological ROS concentrations and prevents the formation of highly reactive and noxious OH radicals.[49] Oxidative stress commonly refers to the imbalance between these natural defense mechanisms and ROS production, leading to an excess of ROS.[50,51]

Previously, the kinetic model KM-SUB-ELF was developed and applied to calculate the chemical exposure-response relationship between PM2.5 and ROS concentrations in the ELF.[13,14,28] The model showed that momentary ROS concentrations can exceed concentrations characteristic for healthy humans (100 nmol L^{-1}) after exposure to PM2.5; furthermore, important redox-active air pollutants as well as cyclic reaction mechanisms with endogenous reaction partners were identified.[14] Recent epidemiological studies with air monitoring and KM-SUB-ELF modeling have found positive associations between long-term exposure to iron, copper, and ROS with the risks of respiratory and cardiovascular diseases.[52−54] A significant positive association was also observed between ROS levels in ELF and COVID-19 incidence.[55]

The metric of momentary ROS concentration is dominated by chemical species with relatively long lifetimes, such as H_2O_2, and foregoes short-lived species like OH that are known to cause damage and oxidative stress.[56,57] While the production mechanisms of H_2O_2 and OH in ELF are closely connected, their yields and concentrations may not. This becomes pertinent, for example, in the presence of transition-metal ions, where Fenton chemistry causes OH formation through decomposition of H_2O_2.[58,59] While the momentary ROS concentration decreases through Fenton chemistry, the overall ROS reactivity and potential to induce oxidative stress may strongly increase.[30] Thus, chemical metrics for oxidative stress are needed that take into account not only the quantity but also the chemical identities of produced ROS.

In this study, the kinetic model KM-SUB-ELF is comprehensively extended and embedded into a new framework for analysis of model output that enables novel insights on the production, interconversion, and scavenging of ROS. The most notable extensions to KM-SUB-ELF are the expansion of the biological antioxidant system by explicit inclusion of the ROS buffering enzymes catalase and SOD, the inclusion of the air pollutant NO_2, and revision of uptake and chemistry of the pollutant O_3. With these additions, the model is now able to capture the fundamental competition between the antioxidant system and the mixture of air pollutants. A new and comprehensive chemical source apportionment pinpoints the chemical species that are most important for production, interconversion, and scavenging of ROS in different pollution scenarios. Based on these learnings, we propose the new chemical metrics of cumulative ROS production rate and H_2O_2-to-OH conversion fraction to represent the potential of air pollution to induce oxidative stress.

METHODS

The kinetic model presented in this study builds on the previously published model KM-SUB-ELF,[14] which is based on the kinetic multilayer model for aerosol surface and bulk chemistry (KM-SUB).[60] KM-SUB-ELF consists of three compartments, the lung gas phase, the surfactant layer of the ELF, and the bulk ELF. The model explicitly treats airflow into and out of the lung, adsorption of gases onto the ELF's surfactant layer, desorption from the surfactant layer, surface-bulk exchange between surfactant layer and bulk ELF, bulk diffusion within the ELF, as well as chemical reactions in the gas and aqueous phases. The temporal evolution of reactants is calculated by solving a system of ordinary differential equations. Table S1 outlines the chemical reactions treated in KM-SUB-ELF, including 23 gas-phase reactions, six reactions in the surfactant layer, and 96 aqueous-phase reactions in the bulk ELF. Rate coefficients for the gas-phase chemical reactions of H_2O_2, HO_2, NO, NO_2, and O_3 are adopted from the Master Chemical Mechanism (MCM).[61,62] The aqueous-phase redox chemistry in the model was validated previously against experimental studies on H_2O_2 and OH formation in surrogate ELF.[14,24,25] H_2O_2 and OH production from SOA are parameterized based on experimental observations.[14,27,63] The ELF is subdivided into six different layers, one surfactant layer containing lipids (1-palmitoyl-2-oleoylglycerol, POG) and a surfactant protein (SP-B), and five bulk layers containing four antioxidants (detailed in the Supporting Information, Section S1) and two antioxidant enzymes (detailed in Section S2). Moreover, a first-order loss reaction of OH is included to account for OH reacting with organic matter that is present in the ELF (Supporting Information, Section S3). Particulate pollutant concentrations in the ELF are derived as described previously (Supporting Information, Section S4).[14] In short, ambient PM2.5 from a 2 h exposure window is deposited into the lung with a deposition fraction of 0.45.[64] Mass fractions of the redox-active constituents in

https://doi.org/10.1021/acs.est.1c03875
Environ. Sci. Technol. 2021, 55, 14069−14079

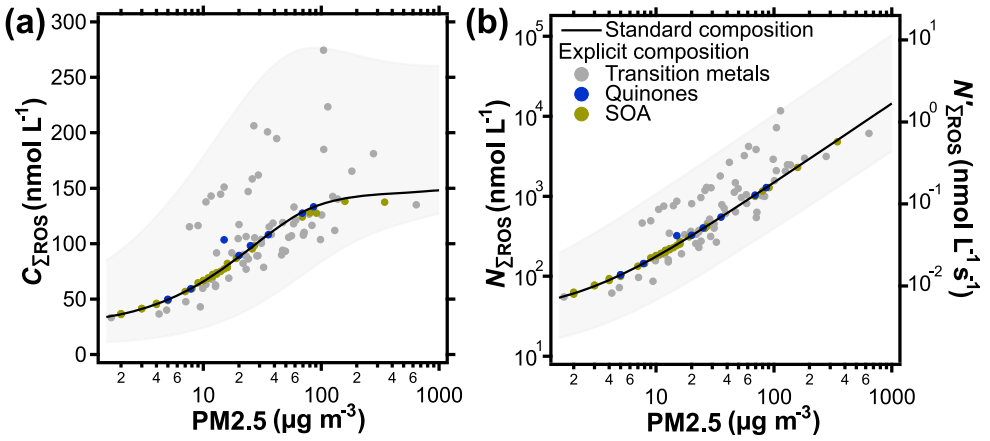

Figure 1. (a) Total ROS concentration, $C_{\sum ROS}$, and (b) cumulative production of ROS, $N_{\sum ROS}$, in the ELF as a function of ambient PM2.5 concentration after a 2 h period of pollutant exposure. The right axis in (b) shows the cumulative ROS production rate ($N'_{\sum ROS}$, Table S4). The solid lines represent a standard PM2.5 composition based on median mass fractions of redox-active constituents of 0.03% copper, 0.8% iron, 0.002% quinones, and 33% SOA. Markers represent explicit PM2.5 composition field data for the indicated redox-active constituents (Tables S5–S7) to illustrate the sensitivity and variance induced by the PM2.5 constituents. Shadings indicate a dynamic range of each concentration metric as a function of PM2.5 composition and concentration of gaseous pollutants.

PM2.5 are obtained from a range of field measurements (Tables S5–S7).[14] Because NO_2 and PM2.5 are often co-emitted, in our calculations the gas-phase concentration of NO_2 is co-varied with PM2.5 concentration with a factor of 1 $\mu g\ m^{-3}$ NO_2 for each $\mu g\ m^{-3}$ PM2.5.[65] Due to the more complex relationship of O_3 and PM2.5, O_3 is treated with a constant concentration of 30 $\mu g\ m^{-3}$ (corresponding to ∼15 ppb at 1 atm, 298 K), irrespective of other pollutant concentrations, to resemble an atmospheric background concentration.[66,67] In Figure 4, three distinct pollutant exposure scenarios are highlighted that have the following characteristics: (1) "clean", with concentrations of 5 $\mu g\ m^{-3}$ PM2.5, 5 $\mu g\ m^{-3}$ NO_2, and 20 $\mu g\ m^{-3}$ O_3; (2) "urban", with 30, 30, and 60 $\mu g\ m^{-3}$; and (3) "megacity", with 300, 300, and 60 $\mu g\ m^{-3}$ for the same pollutants, respectively. Gas exchange between the lungs and the ambient air is included to simulate breathing (detailed in the Supporting Information, Section S5). Volatile vapors partition to the ELF according to Henry's law. Acids and conjugate bases are assumed to maintain equilibrium and the position of the acid–base equilibria is determined using the pKa of the species involved and a pH of 7 (detailed in the Supporting Information, Section S6). A full list of input parameters as used in KM-SUB-ELF is presented in Table S2. The definitions and equations for the calculation of the chemical metrics for oxidative stress are presented in Tables S3 and S4, respectively. To facilitate discussion, we establish a standardized composition of PM2.5, representing median mass fractions of the redox-active PM2.5 constituents copper and iron ions, quinones, and SOA, as determined in field measurements (Tables S5–S7). In figures, standard PM2.5 composition is indicated with solid lines, whereas markers will indicate simulation results using explicit composition data.

RESULTS AND DISCUSSION

Exposure to PM2.5, NO_2, and O_3 results in ROS formation in the ELF. Figure 1a shows the total ROS concentration in the ELF at the end of 2 h of pollutant exposure, $C_{\sum ROS}$, computed using KM-SUB-ELF for a range of pollutant concentrations and for different PM2.5 compositions. We use "∑ROS" to indicate the sum of all ROS treated explicitly in this study, i.e., H_2O_2, O_2^-, HO_2, and OH. The color-coded markers in Figure 1a represent simulation results using mass fractions of single PM2.5 redox-active constituent classes (gray: transition metals, yellow: SOA, blue: quinones) that were obtained in field measurements (Tables S5–S7).[14] In each calculation, the mass fractions of the other constituent classes are kept at their median mass fraction. The median mass fractions of copper and iron ions, quinones, and SOA are determined to be 0.03, 0.8, 0.002, and 33%, respectively (Tables S5–S7). To illustrate the variability in PM2.5 composition, the individual mass fractions obtained from field data are presented in Figure S1. To illustrate the variability in PM2.5 composition, the individual mass fractions obtained from field data are presented in Figure S1.

The black solid line in Figure 1a represents the total momentary ROS concentration, $C_{\sum ROS}$, that results from the standard PM2.5 composition using median mass fractions of all redox-active constituents. The variance pattern of markers around the line in Figure 1a indicates that the transition-metal-ion mass fractions dominate the influence of PM2.5 composition on model output. This is due to both, a strong model sensitivity, and a large variability of transition-metal mass fractions obtained in field measurements (Figure S1). However, the overall model behavior is well represented by the line representing a standardized PM2.5 composition. In the following, we will use this standard composition to assess the effect of ambient PM2.5 concentration on model results. For the purpose of discussion in this study, we categorize pollution levels according to the PM2.5 concentrations as "low" (<10 $\mu g\ m^{-3}$ PM2.5), "typical urban" (10–100 $\mu g\ m^{-3}$ PM2.5), and "very high" (>100 $\mu g\ m^{-3}$ PM2.5) pollution. The model predicts that $C_{\sum ROS}$ ranges from ∼30 nmol L^{-1} at low pollution levels to over 250 nmol L^{-1} at very high pollution. $C_{\sum ROS}$ induced by typical urban exposure is found to range between ∼70 and ∼250 nmol L^{-1}, which is consistent with ROS concentrations measured in exhaled breath condensate of humans.[68,69] In Figure S2, $C_{\sum ROS}$ after 2 h of exposure is compared to the arithmetic mean of $C_{\sum ROS}$ during these 2 h. Qualitatively, both metrics for momentary ROS concentration show very similar behavior, but the time average exhibits

https://doi.org/10.1021/acs.est.1c03875
Environ. Sci. Technol. 2021, 55, 14069–14079

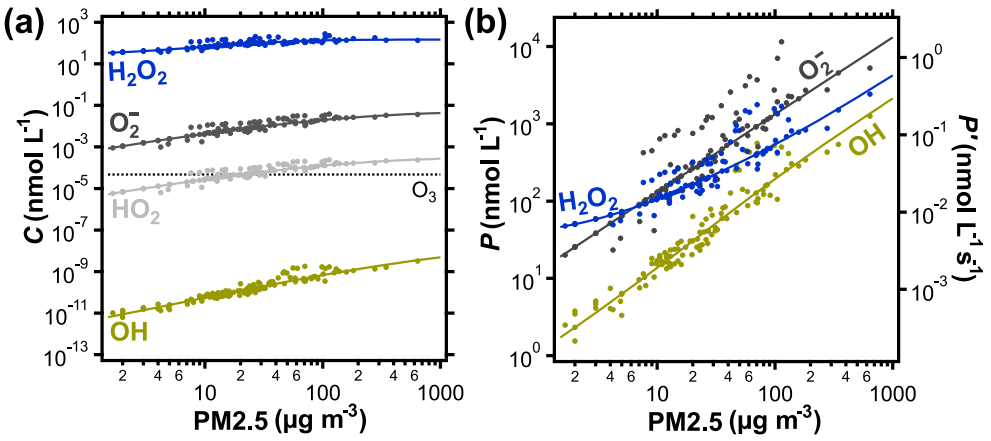

Figure 2. (a) Individual ROS concentrations, *C*, and (b) gross chemical production, *P*, of individual ROS in the ELF as a function of ambient PM2.5 concentration. The right axis in (b) shows the gross chemical production rate of individual ROS (*P*′, Table S4). The solid lines represent a standard PM2.5 composition, and the markers represent explicit PM2.5 compositions derived from field data (Tables S5−S7). C_{O2-} and C_{HO2} in (a) are calculated using acid−base equilibria, as detailed in the Supporting Information, Section S6. In (b), P_{O2-} also includes P_{HO2}. The dotted line in (a) shows the steady-state O_3 concentration in the ELF.

overall slightly lower values due to the initial increase in ROS concentrations.

We note that, to the knowledge of the authors, rates of antioxidant replenishment in ELF have not been reported previously. Kelly et al. showed experimentally that antioxidants do not fully deplete in the ELF of healthy volunteers upon exposure to NO_2.[70] A partial depletion of antioxidants does not affect modeling results (Figure S3) as reactions with the oxidized forms of transition-metal ions and quinones are fast and do not represent a bottleneck for redox cycling in the ELF. Thus, for simplicity, antioxidant replenishment is considered sufficiently fast within the 2 h exposure window and antioxidant concentrations are kept constant in the model calculations. Otherwise, without replenishment of antioxidants, exposure to air pollution with NO_2 concentrations above 100 $\mu g\ m^{-3}$ (corresponding to ∼50 ppb) leads to a spike in $C_{\sum ROS}$ (Figure S3a), caused by full depletion of antioxidants within the 2 h exposure time (Figure S3b). This model result provides evidence for a higher susceptibility to air pollution at critically low antioxidant levels.

Figure 1b introduces the metric of cumulative production of ROS, $N_{\sum ROS}$, as an additional chemical endpoint for the effects of air pollution on human health.

$$N_{\Sigma ROS} = P_{\Sigma ROS} - I_{\Sigma ROS}$$

Here, $P_{\sum ROS}$ is the gross chemical production of ROS (in nmol L^{-1}), i.e., the time-integrated sum of all chemical production terms within the 2 h of exposure. $I_{\sum ROS}$ (in nmol L^{-1}) is the time-integrated sum of ROS molecules that originate from interconversion between individual ROS, and is subtracted to avoid double counting of ROS. Following the solid line of standard PM2.5 composition, $N_{\sum ROS}$ is found to increase linearly with air pollution exposure and ranges from less than 100 nmol L^{-1} at low concentrations of air pollutants, to over 1 μmol L^{-1} at very high concentrations. While the metric $C_{\sum ROS}$ is a measure for stable ROS in the ELF, $N_{\sum ROS}$ accounts for all ROS produced, irrespective of reactivity or lifetime.

Figure 2a shows the contributions of individual species to the total momentary ROS concentration in the ELF. $C_{\sum ROS}$ is found to be dominated by the H_2O_2 concentration, C_{H2O2}, with C_{O2-}, C_{HO2}, and C_{OH} having only negligible contributions.[14] Due to the small contribution of HO_2 to $C_{\sum ROS}$ at pH 7 and the fast interconversion between both species, we use O_2^- for the sum of the HO_2/O_2^- acid−base pair in the following discussions for simplicity. Note that the high and unspecific reactivity of OH with all organic matter in the ELF leads to uncertainty in C_{OH}, which is further detailed in the Supporting Information, Section S3.

Figure 2b outlines the gross chemical production, *P*, of individual ROS in the ELF, which is calculated by time integrating all production terms of the individual species. Over most of the investigated PM2.5 concentration range, O_2^- shows the largest production (10 nmol L^{-1} to 10 μmol L^{-1}), followed by H_2O_2 (40 nmol L^{-1} to 4 μmol L^{-1}), and OH (1 nmol L^{-1} to 2 μmol L^{-1}). These results are consistent with Gonzalez et al.,[71] who found OH production in the range of 0.5−1.5 μmol L^{-1} after 2 h incubation of 1 μmol L^{-1} iron (corresponding to ∼500 $\mu g\ m^{-3}$ PM2.5) in bronchoalveolar lavage fluid.

Figure S4 breaks down the contributions of the individual pollutants PM2.5, NO_2, and O_3 to the gross chemical productions of ROS shown in Figure 2b. Production of O_2^- and OH can be largely attributed to PM2.5 (Figure S4a), whereas H_2O_2 is produced in significant quantity from O_3 reacting with unsaturated lipids in the surfactant layer (R27, Table S1 and Figure S4b). Thus, H_2O_2 dominates gross chemical production of ROS at low ambient pollutant concentrations because of the constant O_3 background concentration, which is assigned irrespective of PM2.5 and NO_2 levels. Accordingly, at a PM2.5 concentration of 7 $\mu g\ m^{-3}$, production of O_2^- surpasses production of H_2O_2. We note that, to the knowledge of the authors, H_2O_2 yield from surfactant ozonolysis in the ELF has not been reported previously. H_2O_2 yields from gas-phase ozonolysis of small alkenes in the presence of bulk water are found between 3 and 24%.[43] A compound that closely resembles fatty acid residues in mono-unsaturated lipids is methyl oleate, which showed an H_2O_2 yield of 17% and was taken as a reference for this study.[72] The exact yield of H_2O_2 will also depend on the water content in the lipid layer of the ELF, which determines Criegee intermediate fate, and warrants further investigation.[43,72]

Compared to momentary concentrations of individual ROS, which span 10−12 orders of magnitude (Figure 2a), the individual gross chemical productions are within about 2

https://doi.org/10.1021/acs.est.1c03875
Environ. Sci. Technol. 2021, 55, 14069−14079

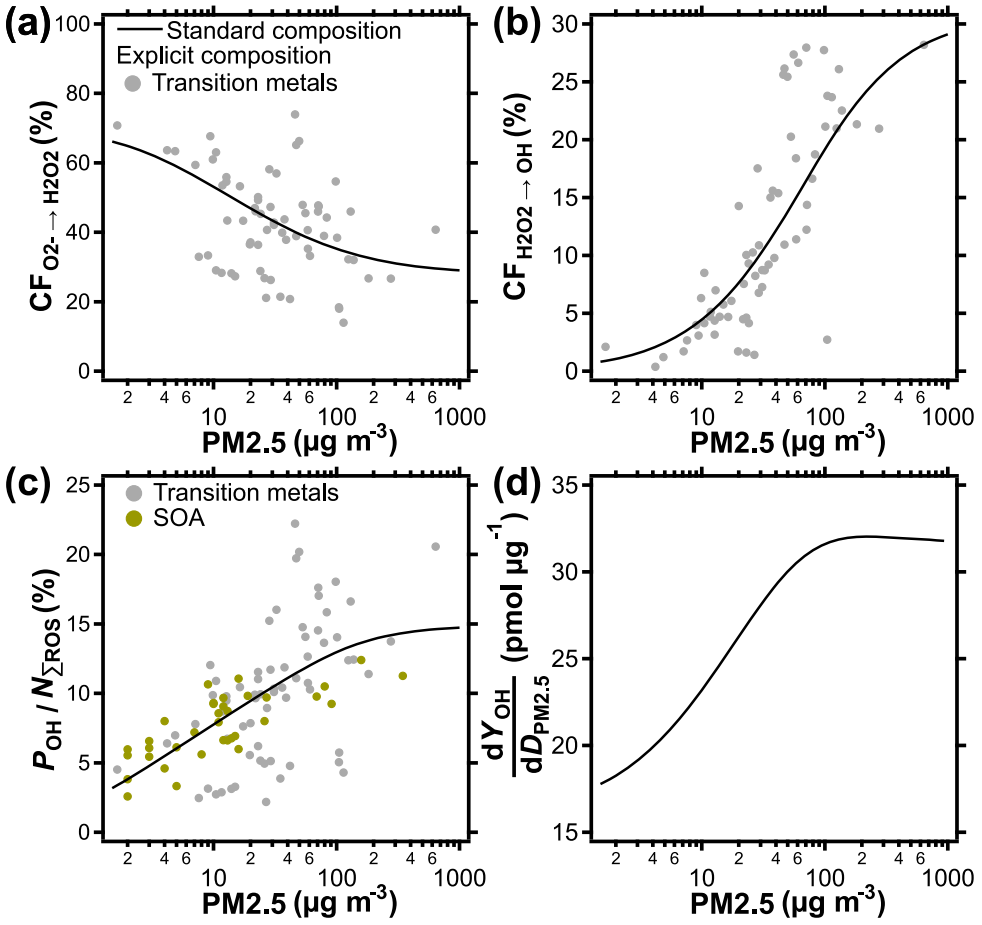

Figure 3. (a) ROS conversion fractions (CF) for the conversion of O_2^- to H_2O_2 and (b) the conversion of H_2O_2 to OH as a function of ambient PM2.5 concentration. (c) OH fraction of the total cumulative ROS production expressed as a percentage and (d) the change in OH yield per change in PM2.5 dose in the ELF as a function of PM2.5 concentration. CF represents the fraction of the total produced ROS that undergo the indicated conversion pathway as opposed to being scavenged, exhaled, or accumulated in the ELF within 2 h of simulation time. The lines represent a standard PM2.5 composition; the markers in (a–c) show the effect of using explicit PM2.5 composition data (Table S5).

orders of magnitude from each other at low pollutant concentrations, and within about 1 order of magnitude at higher pollutant concentrations (Figure 2b). This finding can be attributed to the chain of ROS interconversions in the ELF: O_2^- is often produced initially and then successively converted into H_2O_2 and OH. The decreasing disparity between individual production terms with increasing PM2.5 concentration in Figure 2b suggests that ROS are interconverted more efficiently at higher pollution levels.

To illustrate shifts in ROS interconversion patterns, a chemical pathway analysis is conducted and the results are displayed in Figure 3a,b. ROS conversion fractions (CF), i.e., the percentage fraction of a ROS that is chemically converted to other ROS and not scavenged, exhaled, or accumulated, are presented as a function of pollutant concentrations. The term scavenging is used for chemical reactions that convert ROS into largely unreactive products such as H_2O or O_2. Figure 3a,b shows the fraction of O_2^- converted to H_2O_2 ($CF_{O2-\rightarrow H2O2}$) and the fraction of H_2O_2 converted to OH ($CF_{H2O2\rightarrow OH}$), respectively. In analogy to Figure 1, the solid lines represent standard PM2.5 composition, whereas explicit composition markers illustrate the sensitivity and variance induced by PM2.5 constituents. Explicit composition markers for SOA and quinones are omitted from Figure 3a,b as these compounds show no, or only negligible contribution to ROS interconversion, respectively. The fraction of O_2^- converted to H_2O_2 is high with >50% at low pollution, falls below 50% at typical urban pollution levels, and stabilizes at ∼30% at very high pollution. The drop in $CF_{O2-\rightarrow H2O2}$ can be attributed to transition metals becoming the more important reaction partner of O_2^- compared to antioxidants and enzymes. The mixture of SOD and ascorbate in the ELF scavenges about 33% of O_2^- and converts about 66% of O_2^- to H_2O_2. The ratio of scavenged to converted is generally higher for transition metals, as well as depends on the iron to copper ratio, as indicated by the scatter of markers in Figure 3a. This effect will be further detailed in Figure 4d.

The terminal element in the ROS interconversion chain is the conversion of H_2O_2 to the OH radical. OH reacts quickly, at or near site of formation, and with nearly all molecules in the ELF, and may directly cause damage to biomolecules, cells, and tissues.[30,49] At low PM2.5 concentrations, the fraction of H_2O_2 converted to OH is low, ranging from 0.5 to 4% (Figure 3b). However, this fraction shows a strong nonlinear increase from 4 to 19% at typical urban pollution levels, and may reach up to 29% at very high pollution according to the model. The nonlinear increase in $CF_{H2O2\rightarrow OH}$ with PM2.5 concentration is due to competition of catalase and transition metals for reaction with H_2O_2. Catalase scavenges H_2O_2 at a constant rate. Its importance diminishes as the rate of the Fenton

https://doi.org/10.1021/acs.est.1c03875
Environ. Sci. Technol. 2021, 55, 14069−14079

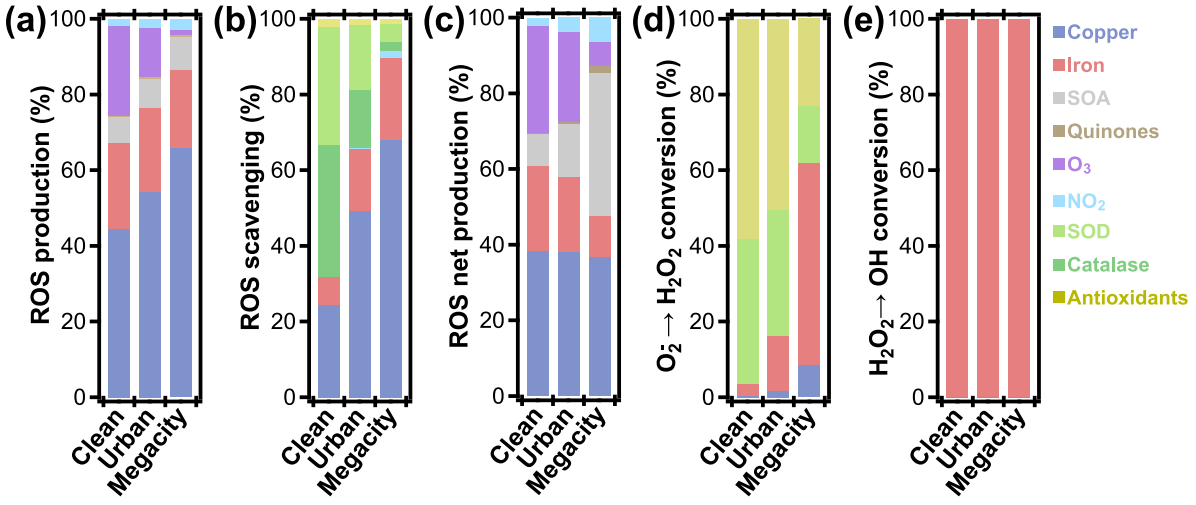

Figure 4. Relative contributions of pollutants, enzymes, and antioxidants to chemical production, scavenging, and conversion of ROS in ELF for three characteristic pollution scenarios (clean, urban, megacity; see the Methods section): (a) ROS production, (b) ROS scavenging, (c) ROS net production, (d) O_2^--to-H_2O_2 conversion, and (e) H_2O_2-to-OH conversion. Concentrations of individual PM2.5 constituents are determined based on a standard PM2.5 composition obtained from field observations (Tables S5−S7).

reaction increases toward high PM2.5 concentrations. When PM2.5 exposure is highest, the effect of catalase is negligible and $CF_{H2O2\rightarrow OH}$ identical to the OH yield of the Fenton reaction, which is about 30% in the chemical mechanism used in this study (Table S1).

In conclusion, while the fraction of O_2^- that is converted to H_2O_2 decreases by a factor of ∼2 over the investigated pollution range, the conversion fraction of H_2O_2 to OH increases by a factor of ∼50. Figure 3c shows the joint effect of ROS production and interconversion by calculating the share of OH production, P_{OH}, within the cumulative ROS production, $N_{\sum ROS}$, as a function of pollutant concentration. At low pollutant concentrations, this contribution of OH to $N_{\sum ROS}$ is small with only ∼5%. The value increases to 15% toward very high pollution levels and may even reach 20% for specific PM2.5 compositions. This change in kinetic regime may have drastic implications on the health effects of PM2.5 as more of the highly reactive OH is created, both absolutely (Figure 2b) and relatively (Figure 3c), with increasing pollution levels. The tipping point for this regime change lies in the range of typical urban pollution in this simulation (Figure 3b).

Figure 3d shows the incremental increase in OH yield, $dY_{OH}/dD_{PM2.5}$, plotted against PM2.5 concentration. Here, Y_{OH} is the OH yield (pmol) and $D_{PM2.5}$ (μg) is the dose of PM2.5 inhaled and deposited in the ELF. At low pollutant concentrations, $dY_{OH}/dD_{PM2.5}$ is around 20 pmol μg^{-1}. In the range of typical urban pollutant concentrations, however, it increases steadily, suggesting that ROS buffering becomes less effective, and PM2.5 more harmful. At a pollutant concentration of 100 $\mu g\ m^{-3}$, the incremental OH yield reaches a maximum level around 30 pmol μg^{-1}. The increase of $dY_{OH}/dD_{PM2.5}$ shows that the ROS buffering capacity of the physiological antioxidant defense is exhausted at high PM2.5 levels.

To gain insight into the chemical species and reactions responsible for this change in kinetic regime, ROS production, scavenging, and conversions are apportioned to constituents of air pollution, enzymes, and antioxidants in the ELF (Figure 4). As shown previously,[14] copper and iron ions are found to be the main sources, i.e., gross producers of ROS in the ELF, largely independent of pollutant concentration (Figure 4a). Chemical reactions involving transition-metal ions give rise to ca. 70−90% of all initial ROS formed in the ELF by reduction of molecular oxygen O_2 to O_2^- (R48 and R54, Table S1), whereas chemical reactions involving O_3, NO_2, and SOA together are responsible for the remaining ca. 10−30%. O_3 constitutes a significant ROS source in the "clean" and "urban" scenarios but is less important in the "megacity" scenario.

Figure 4b details the efficacy of all explicit ROS scavengers in the ELF. Note that, while the reaction of OH with antioxidants is counted here toward ROS scavenging, the unspecific loss of OH is not, because these reactions can retain the unpaired electron (e.g., H-abstraction: RH + OH → R• + H_2O). These reactions may rather result in physiological damage and initiate chain propagation reactions such as lipid peroxidation.[73] The model finds that the reactions of antioxidants with OH make up 7% of total OH loss in the ELF, which corresponds to <2% of the total ROS scavenging. The most potent endogenous ROS sinks include the enzymatic scavenging of one equivalent of O_2^- in the disproportionation by superoxide dismutase (SOD, R124, Table S1), and the scavenging of H_2O_2 by catalase (R125, Table S1). At very low pollutant concentrations, 70% of all scavenged ROS can be attributed to reactions of enzymes, reflecting efficient ROS buffering by endogenous molecules in the ELF. However, dissolved copper and iron can also scavenge ROS (R42, 44, 51, 56, Table S1), which becomes increasingly important at higher pollutant concentrations. In the "urban" exposure scenario, already about 60% of ROS scavenging is attributed to these transition metals, whereas under "megacity" conditions this number reaches 90%. This signifies the multifaceted role of transition-metal ions in the ELF, i.e., not only inducing formation, but also loss of ROS.

To account for such multifaceted roles of pollutants, the net production of ROS from individual sources is presented in Figure 4c. Net productions are computed using the number of ROS molecules produced by a pollutant, subtracted by the number of ROS molecules scavenged in chemical reactions with that pollutant. With these considerations, the model

https://doi.org/10.1021/acs.est.1c03875
Environ. Sci. Technol. 2021, 55, 14069−14079

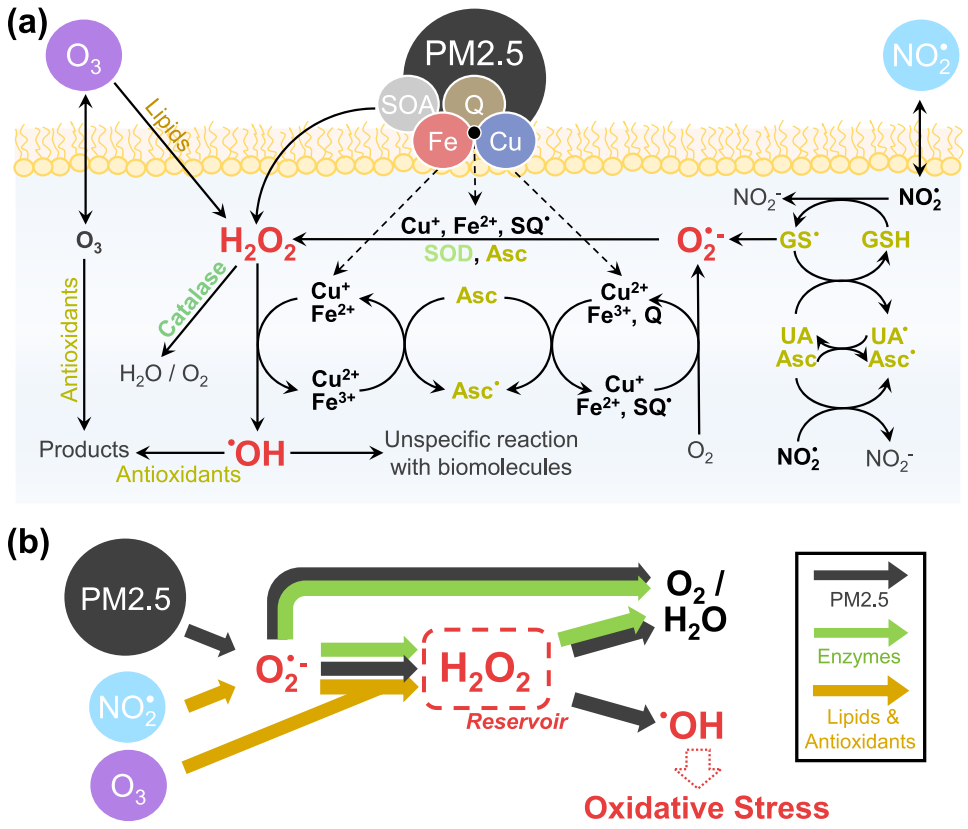

Figure 5. (a) Production, interconversion, and scavenging of reactive oxygen species (ROS) by air pollutants and endogenous molecules in the epithelial lining fluid (ELF). Organic and inorganic constituents of fine particulate matter (PM2.5) can produce, convert, and scavenge ROS. Enzymes (catalase; superoxide dismutase, SOD) intercept ROS through the disproportionation of O_2^- and the decomposition of H_2O_2 (green). Antioxidants (ascorbate; glutathione, GSH; uric acid, UA; α-tocopherol, α-Toc) intercept OH, O_2^-, and H_2O_2, but the reaction of antioxidants and surfactant lipids with NO_2 and O_3 can also produce ROS (yellow). Note that PM2.5 constituents are able to convert the relatively stable reservoir species H_2O_2 into the highly reactive OH radical, which may cause oxidative stress (distress) and physiological damage.[30,79] (b) Schematic summary of the main reaction pathways.

predicts that transition-metal ions are responsible for ca. 50−60% of all ROS. While O_3 contributes ∼30% in "clean" conditions, the contribution is reduced to less than 10% under highly polluted "megacity" conditions, where SOA becomes an important net source of ROS. Quinones are found to have a small effect on ROS formation in "megacity" conditions. Taken together, PM2.5 constituents are responsible for ∼70% of all net ROS production in "clean" conditions. This share increases to ∼80% in highly polluted "megacity" conditions.

The model simulations show that about half of the produced O_2^- is scavenged during its lifetime in the ELF while the other half is converted into H_2O_2. Figure 4d shows that SOD (R124, Table S1) and antioxidants (R73, R74, Table S1) are the main drivers of this conversion and are responsible for over 90 and 80% of the H_2O_2 formation from O_2^- in "clean" and "urban" environments, respectively. However, under highly polluted "megacity" conditions, transition-metal ions in PM2.5 supersede endogenous molecules in the conversion of O_2^- into H_2O_2, which signifies another facet in the redox chemistry of transition metals in the ELF.

While multiple species in the ELF convert O_2^- into H_2O_2, the model suggests that the conversion of H_2O_2 to OH almost exclusively involves the PM2.5 constituent iron (Figure 4e). This reaction converts a very stable form of ROS into a very reactive and noxious ROS, thereby strongly increasing overall ROS reactivity. Thus, the ions of the two transition metals iron and copper differ in their role for ROS formation and interconversion in the ELF: copper contributes more to initial ROS formation by reduction of O_2 to O_2^-, while iron is more important for increasing ROS reactivity by conversion of H_2O_2 into OH radicals.[30]

Figure 5a illustrates the main reaction pathways of ROS formation, interconversion, and scavenging in the ELF. Figure 5b summarizes the insights from chemical pathway analysis and apportionment as presented in Figures 1−4 in a schematic representation. In this study, we focus on OH as the main source of oxidative stress due to its unspecific, high reactivity with any biomolecule (e.g., lipids, proteins). In contrast, such reactivity is not known for other species, including O_2^- and H_2O_2.[74] While O_2^- has been related to health effects, not many reaction rates with organic and biomolecules, other than especially redox-active substances (e.g., (semi-)quinones, thiols) and nitric oxide, are reported in the literature.[39,75−78] Thus, O_2^- may act predominantly as a transient species in the ROS interconversion chain. Similarly, H_2O_2 has been implicated as a mediator and marker for disease.[29,30,68,79] While the model suggests that C_{H2O2} exceeds healthy levels of ∼100 nmol L^{-1} after exposure to PM2.5, H_2O_2 is much less reactive than other ROS, can diffuse across cells and tissues, and allows for scavenging by antioxidant enzymes.[30,80,81] In Figure 5b, H_2O_2 is thus presented as a reservoir for radical species. This reservoir is pivotal in the interception of ROS by natural antioxidants and enzymes, which maintain physiological ROS concentration levels.[30,81] ROS interception

https://doi.org/10.1021/acs.est.1c03875
Environ. Sci. Technol. 2021, 55, 14069−14079

includes the conversion of O_2^- into H_2O_2 and the scavenging of O_2^- and H_2O_2 by antioxidants and enzymes.[30,75] The kinetic model shows that the ELF defense mechanism against oxidative stress acts by antioxidant- and enzyme-driven conversion of the O_2^- radical into H_2O_2, followed by enzymatic decomposition of the reservoir species to avoid conversion into the highly reactive and noxious OH radical.

In Figure 5b, the interception of ROS by natural defense mechanisms is indicated with green arrows. At PM2.5 concentrations under 10 $\mu g\ m^{-3}$, ROS buffering is efficient and leads to low yields of OH. At PM2.5 concentrations above 10 $\mu g\ m^{-3}$, transition-metal ions supersede SOD in its ability to intercept O_2^-. Furthermore, transition-metal ions compete with catalase for H_2O_2. When catalase is unable to remove H_2O_2 fast enough, substantial OH production occurs through Fenton and Fenton-like reactions. As OH cannot be effectively intercepted, Fenton chemistry circumvents ROS scavenging and reduces the ROS interception efficiency of the ELF. Thus, exposure to PM2.5 can lead to a shift from the enzyme-controlled ROS buffering regime to the PM2.5-controlled OH radical production regime, leading to increased ROS reactivity and oxidative stress. This switch in the kinetic regime to a state of diminished ROS buffering efficiency may already occur at ambient PM2.5 concentrations >10 $\mu g\ m^{-3}$, emphasizing the need for regulators to more strictly follow the WHO air quality guideline for PM2.5 concentration, which, coincidentally, is set to 10 $\mu g\ m^{-3}$.[82] This is of particular importance in urban areas, in which PM2.5 concentrations often range between 10 and 100 $\mu g\ m^{-3}$, as slight decreases in exposure levels may be especially effective in this pollution range. We note however that, to date, it remains unclear whether a safe PM2.5 pollutant concentration, at which no health effects of air pollution could be observed, exists.[1] Although the calculated OH productions at low pollutant concentration in this study are comparatively small, they remain nonzero.

The calculations presented in this study assume a stable, physiological pH as found in healthy individuals. In certain diseased states, however, the pH of the ELF may be decreased,[83,84] potentially exacerbating ROS formation through increased transition-metal solubility[85] or reduced enzyme activity.[86] Moreover, α-hydroxyhydroperoxides are suggested to increasingly produce H_2O_2 at low pH.[87] To date, the exact product yields of the Fenton reaction remain unclear;[88] however, at lower pH, the Fenton reaction may increasingly yield OH,[89,90] which may further facilitate oxidative stress. For efficient policy-making, future studies will have to further refine the conditions, i.e., pollutant levels and composition, under which OH production in the ELF will be strongly enhanced. Factors adding uncertainty to the model are the role of ELF pH, transition-metal coordination and solubility, ELF replenishment and antioxidant recovery, OH and H_2O_2 yields from organic molecules and SOA, as well as concentrations of antioxidant enzymes.

In conclusion, our results suggest that the presence of PM2.5 may increasingly trigger oxidative stress in the ELF not only through an increase in overall ROS concentrations[47] but also by increasingly producing the most noxious form of ROS, OH, in Fenton and Fenton-like reactions. Both processes, ROS production and H_2O_2-to-OH conversion, contribute to the exposure of biomolecules and tissues to highly reactive OH. Chemical metrics that assess the potential of air pollution to induce oxidative stress must capture both, the quantity and the overall reactivity of ROS. Hence, in this study, we introduce the metrics of cumulative ROS production (Figure 1b) and H_2O_2-to-OH conversion fraction (Figure 3b). It remains open how these metrics correlate with epidemiological data and disease endpoints, which will be subject to future studies.

■ ASSOCIATED CONTENT

Supporting Information

The Supporting Information is available free of charge at https://pubs.acs.org/doi/10.1021/acs.est.1c03875.

ELF antioxidant concentrations (S1); ELF enzymatic reactions (S2); OH reactions with unspecified organic matter and estimated OH lifetime in the ELF (S3); particulate pollutant concentrations in the ELF (S4); gas-phase pollutant concentrations in the ELF (S5); acid dissociation (S6); pH of the ELF (S7); chemical reaction mechanism (Table S1); input parameters to the KM-SUB-ELF model (Table S2); list of symbols and definitions (Table S3); mathematical formulas used to calculate ROS metrics (Table S4); PM2.5 and transition-metal mass fractions (Table S5); PM2.5 and secondary organic aerosol (SOA) mass fractions (Table S6); PM2.5 and quinone mass fractions (Table S7); mass fractions of all redox-active PM2.5 constituents quantified in field data (Figure S1); endpoint and average ROS concentration, $C_{\Sigma ROS}$, in the ELF as a function of PM2.5 concentration (Figure S2); ROS concentration, $C_{\Sigma ROS}$, and antioxidant consumption rate as a function of pollutant concentration (Figure S3); gross chemical production of individual ROS in the ELF as a function of the concentration of three distinct pollutants (Figure S4); O_3 and NO_2 concentrations and saturation point in the ELF as a function of ambient pollutant concentration (Figure S5); and pH 4 sensitivity study (Figure S6) (PDF)

■ AUTHOR INFORMATION

Corresponding Author

Thomas Berkemeier − *Multiphase Chemistry Department, Max Planck Institute for Chemistry, 55128 Mainz, Germany;* orcid.org/0000-0001-6390-6465; Email: t.berkemeier@mpic.de

Authors

Steven Lelieveld − *Multiphase Chemistry Department, Max Planck Institute for Chemistry, 55128 Mainz, Germany*

Jake Wilson − *Multiphase Chemistry Department, Max Planck Institute for Chemistry, 55128 Mainz, Germany;* orcid.org/0000-0002-2342-6966

Eleni Dovrou − *Multiphase Chemistry Department, Max Planck Institute for Chemistry, 55128 Mainz, Germany*

Ashmi Mishra − *Multiphase Chemistry Department, Max Planck Institute for Chemistry, 55128 Mainz, Germany*

Pascale S. J. Lakey − *Department of Chemistry, University of California, Irvine, Irvine, California 92697, United States;* orcid.org/0000-0003-2923-4073

Manabu Shiraiwa − *Department of Chemistry, University of California, Irvine, Irvine, California 92697, United States;* orcid.org/0000-0003-2532-5373

Ulrich Pöschl − *Multiphase Chemistry Department, Max Planck Institute for Chemistry, 55128 Mainz, Germany;* orcid.org/0000-0003-1412-3557

Complete contact information is available at:

https://pubs.acs.org/10.1021/acs.est.1c03875

Funding

Open access funded by Max Planck Society.

Notes

The authors declare no competing financial interest.

■ ACKNOWLEDGMENTS

This work was funded by the Max Planck Graduate Center with the Johannes Gutenberg University (MPGC) and the Max Planck Society (MPG). The authors thank A. Filippi, G. Lammel, J. Lelieveld, K. Lucas, and H. Tong for stimulating discussions and D. Jack for helpful advice on figure design. M.S. acknowledges funding from the Health Effects Institute (No. 4964-RFA17-3/18-6).

■ REFERENCES

(1) Burnett, R.; Chen, H.; Szyszkowicz, M.; Fann, N.; Hubbell, B.; Pope, C. A.; Apte, J. S.; Brauer, M.; Cohen, A.; Weichenthal, S.; Coggins, J.; Di, Q.; Brunekreef, B.; Frostad, J.; Lim, S. S.; Kan, H.; Walker, K. D.; Thurston, G. D.; Hayes, R. B.; Lim, C. C.; Turner, M. C.; Jerrett, M.; Krewski, D.; Gapstur, S. M.; Diver, W. R.; Ostro, B.; Goldberg, D.; Crouse, D. L.; Martin, R. V.; Peters, P.; Pinault, L.; Tjepkema, M.; van Donkelaar, A.; Villeneuve, P. J.; Miller, A. B.; Yin, P.; Zhou, M.; Wang, L.; Janssen, N. A. H.; Marra, M.; Atkinson, R. W.; Tsang, H.; Quoc Thach, T.; Cannon, J. B.; Allen, R. T.; Hart, J. E.; Laden, F.; Cesaroni, G.; Forastiere, F.; Weinmayr, G.; Jaensch, A.; Nagel, G.; Concin, H.; Spadaro, J. V. Global Estimates of Mortality Associated with Long-Term Exposure to Outdoor Fine Particulate Matter. *Proc. Natl. Acad. Sci. U.S.A.* **2018**, *115*, 9592−9597.

(2) Lelieveld, J.; Pozzer, A.; Pöschl, U.; Fnais, M.; Haines, A.; Münzel, T. Loss of Life Expectancy from Air Pollution Compared to Other Risk Factors: A Worldwide Perspective. *Cardiovasc. Res.* **2020**, *116*, 1910−1917.

(3) Landrigan, P. J.; Fuller, R.; Acosta, N. J. R.; Adeyi, O.; Arnold, R.; Basu, N. Nil.; Baldé, A. B.; Bertollini, R.; Bose-O'Reilly, S.; Boufford, J. I.; Breysse, P. N.; Chiles, T.; Mahidol, C.; Coll-Seck, A. M.; Cropper, M. L.; Fobil, J.; Fuster, V.; Greenstone, M.; Haines, A.; Hanrahan, D.; Hunter, D.; Khare, M.; Krupnick, A.; Lanphear, B.; Lohani, B.; Martin, K.; Mathiasen, K. V.; McTeer, M. A.; Murray, C. J. L.; Ndahimananjara, J. D.; Perera, F.; Potočnik, J.; Preker, A. S.; Ramesh, J.; Rockström, J.; Salinas, C.; Samson, L. D.; Sandilya, K.; Sly, P. D.; Smith, K. R.; Steiner, A.; Stewart, R. B.; Suk, W. A.; van Schayck, O. C. P.; Yadama, G. N.; Yumkella, K.; Zhong, M. The Lancet Commission on Pollution and Health. *Lancet* **2018**, *391*, 462−512.

(4) Burnett, R. T.; Pope, C. A.; Ezzati, M.; Olives, C.; Lim, S. S.; Mehta, S.; Shin, H. H.; Singh, G.; Hubbell, B.; Brauer, M.; Anderson, H. R.; Smith, K. R.; Balmes, J. R.; Bruce, N. G.; Kan, H.; Laden, F.; Prüss-Ustün, A.; Turner, M. C.; Gapstur, S. M.; Diver, W. R.; Cohen, A. An Integrated Risk Function for Estimating the Global Burden of Disease Attributable to Ambient Fine Particulate Matter Exposure. *Environ. Health Perspect.* **2014**, *122*, 397−403.

(5) Apte, J. S.; Marshall, J. D.; Cohen, A. J.; Brauer, M. Addressing Global Mortality from Ambient PM $_{2.5}$. *Environ. Sci. Technol.* **2015**, *49*, 8057−8066.

(6) Cohen, A. J.; Brauer, M.; Burnett, R.; Anderson, H. R.; Frostad, J.; Estep, K.; Balakrishnan, K.; Brunekreef, B.; Dandona, L.; Dandona, R.; Feigin, V.; Freedman, G.; Hubbell, B.; Jobling, A.; Kan, H.; Knibbs, L.; Liu, Y.; Martin, R.; Morawska, L.; Pope, C. A.; Shin, H.; Straif, K.; Shaddick, G.; Thomas, M.; van Dingenen, R.; van Donkelaar, A.; Vos, T.; Murray, C. J. L.; Forouzanfar, M. H. Estimates and 25-Year Trends of the Global Burden of Disease Attributable to Ambient Air Pollution: An Analysis of Data from the Global Burden of Diseases Study 2015. *Lancet* **2017**, *389*, 1907−1918.

(7) COMEAP (Committee on the Medical Effects of Air Pollutants). Associations of Long-Term Average Concentrations of Nitrogen Dioxide with Mortality, 2018.

(8) Turner, M. C.; Jerrett, M.; Pope, C. A.; Krewski, D.; Gapstur, S. M.; Diver, W. R.; Beckerman, B. S.; Marshall, J. D.; Su, J.; Crouse, D. L.; Burnett, R. T. Long-Term Ozone Exposure and Mortality in a Large Prospective Study. *Am. J. Respir. Crit. Care Med.* **2016**, *193*, 1134−1142.

(9) Peng, R. D.; Bell, M. L.; Geyh, A. S.; McDermott, A.; Zeger, S. L.; Samet, J. M.; Dominici, F. Emergency Admissions for Cardiovascular and Respiratory Diseases and the Chemical Composition of Fine Particle Air Pollution. *Environ. Health Perspect.* **2009**, *117*, 957−963.

(10) Sarnat, J. A.; Marmur, A.; Klein, M.; Kim, E.; Russell, A. G.; Sarnat, S. E.; Mulholland, J. A.; Hopke, P. K.; Tolbert, P. E. Fine Particle Sources and Cardiorespiratory Morbidity: An Application of Chemical Mass Balance and Factor Analytical Source-Apportionment Methods. *Environ. Health Perspect.* **2008**, *116*, 459−466.

(11) Krall, J. R.; Mulholland, J. A.; Russell, A. G.; Balachandran, S.; Winquist, A.; Tolbert, P. E.; Waller, L. A.; Sarnat, S. E. Associations between Source-Specific Fine Particulate Matter and Emergency Department Visits for Respiratory Disease in Four U.S. Cities. *Environ. Health Perspect.* **2017**, *125*, 97−103.

(12) Baxter, L. K.; Duvall, R. M.; Sacks, J. Examining the Effects of Air Pollution Composition on within Region Differences in PM2.5 Mortality Risk Estimates. *J. Expo. Sci. Environ. Epidemiol.* **2013**, *23*, 457−465.

(13) Weichenthal, S.; Lavigne, E.; Evans, G.; Pollitt, K.; Burnett, R. T. Ambient PM2.5 and Risk of Emergency Room Visits for Myocardial Infarction: Impact of Regional PM2.5 Oxidative Potential: A Case-Crossover Study. *Environ. Health* **2016**, *15*, 46.

(14) Lakey, P. S. J.; Berkemeier, T.; Tong, H.; Arangio, A. M.; Lucas, K.; Pöschl, U.; Shiraiwa, M. Chemical Exposure-Response Relationship between Air Pollutants and Reactive Oxygen Species in the Human Respiratory Tract. *Sci. Rep.* **2016**, *6*, No. 32916.

(15) Münzel, T.; Gori, T.; Al-Kindi, S.; Deanfield, J.; Lelieveld, J.; Daiber, A.; Rajagopalan, S. Effects of Gaseous and Solid Constituents of Air Pollution on Endothelial Function. *Eur. Heart J.* **2018**, *39*, 3543−3550.

(16) Yang, A.; Wang, M.; Eeftens, M.; Beelen, R.; Dons, E.; Leseman, D. L. A. C.; Brunekreef, B.; Cassee, F. R.; Janssen, N. A. H.; Hoek, G. Spatial Variation and Land Use Regression Modeling of the Oxidative Potential of Fine Particles. *Environ. Health Perspect.* **2015**, *123*, 1187−1192.

(17) Gao, D.; Ripley, S.; Weichenthal, S.; Godri Pollitt, K. J. Ambient Particulate Matter Oxidative Potential: Chemical Determinants, Associated Health Effects, and Strategies for Risk Management. *Free Radical Biol. Med.* **2020**, *151*, 7−25.

(18) Sarnat, S. E.; Chang, H. H.; Weber, R. J. Ambient PM2.5 and Health: Does PM 2.5 Oxidative Potential Play a Role? *Am. J. Respir. Crit. Care Med.* **2016**, *194*, 530−531.

(19) Bates, J. T.; Weber, R. J.; Abrams, J.; Verma, V.; Fang, T.; Klein, M.; Strickland, M. J.; Sarnat, S. E.; Chang, H. H.; Mulholland, J. A.; Tolbert, P. E.; Russell, A. G. Reactive Oxygen Species Generation Linked to Sources of Atmospheric Particulate Matter and Cardiorespiratory Effects. *Environ. Sci. Technol.* **2015**, *49*, 13605−13612.

(20) Künzli, N.; Mudway, I. S.; Götschi, T.; Shi, T.; Kelly, F. J.; Cook, S.; Burney, P.; Forsberg, B.; Gauderman, J. W.; Hazenkamp, M. E.; Heinrich, J.; Jarvis, D.; Norbäck, D.; Payo-Losa, F.; Poli, A.; Sunyer, J.; Borm, P. J. A. Comparison of Oxidative Properties, Light Absorbance, and Total and Elemental Mass Concentration of Ambient PM $_{2.5}$ Collected at 20 European Sites. *Environ. Health Perspect.* **2006**, *114*, 684−690.

(21) Janssen, N. A. H.; Yang, A.; Strak, M.; Steenhof, M.; Hellack, B.; Gerlofs-Nijland, M. E.; Kuhlbusch, T.; Kelly, F.; Harrison, R.; Brunekreef, B.; Hoek, G.; Cassee, F. Oxidative Potential of Particulate Matter Collected at Sites with Different Source Characteristics. *Sci. Total Environ.* **2014**, *472*, 572−581.

(22) Crobeddu, B.; Baudrimont, I.; Deweirdt, J.; Sciare, J.; Badel, A.; Camproux, A.-C.; Bui, L. C.; Baeza-Squiban, A. Lung Antioxidant Depletion: A Predictive Indicator of Cellular Stress Induced by Ambient Fine Particles. *Environ. Sci. Technol.* **2020**, *54*, 2360−2369.
(23) Weichenthal, S.; Lavigne, E.; Evans, G.; Pollitt, K.; Burnett, R. T. Fine Particulate Matter and Emergency Room Visits for Respiratory Illness. Effect Modification by Oxidative Potential. *Am. J. Respir. Crit. Care Med.* **2016**, *194*, 577−586.
(24) Charrier, J. G.; McFall, A. S.; Richards-Henderson, N. K.; Anastasio, C. Hydrogen Peroxide Formation in a Surrogate Lung Fluid by Transition Metals and Quinones Present in Particulate Matter. *Environ. Sci. Technol.* **2014**, *48*, 7010−7017.
(25) Charrier, J. G.; Anastasio, C. Impacts of Antioxidants on Hydroxyl Radical Production from Individual and Mixed Transition Metals in a Surrogate Lung Fluid. *Atmos. Environ.* **2011**, *45*, 7555−7562.
(26) Tong, H.; Lakey, P. S. J.; Arangio, A. M.; Socorro, J.; Kampf, C. J.; Berkemeier, T.; Brune, W. H.; Pöschl, U.; Shiraiwa, M. Reactive Oxygen Species Formed in Aqueous Mixtures of Secondary Organic Aerosols and Mineral Dust Influencing Cloud Chemistry and Public Health in the Anthropocene. *Faraday Discuss.* **2017**, *200*, 251−270.
(27) Tong, H.; Arangio, A. M.; Lakey, P. S. J.; Berkemeier, T.; Liu, F.; Kampf, C. J.; Brune, W. H.; Pöschl, U.; Shiraiwa, M. Hydroxyl Radicals from Secondary Organic Aerosol Decomposition in Water. *Atmos. Chem. Phys.* **2016**, *16*, 1761−1771.
(28) Fang, T.; Lakey, P. S. J.; Weber, R. J.; Shiraiwa, M. Oxidative Potential of Particulate Matter and Generation of Reactive Oxygen Species in Epithelial Lining Fluid. *Environ. Sci. Technol.* **2019**, *53*, 12784−12792.
(29) Sies, H.; Jones, D. P. Reactive Oxygen Species (ROS) as Pleiotropic Physiological Signalling Agents. *Nat. Rev. Mol. Cell Biol.* **2020**, *21*, 363−383.
(30) Sies, H.; Berndt, C.; Jones, D. P. Oxidative Stress. *Annu. Rev. Biochem.* **2017**, *86*, 715−748.
(31) Saffari, A.; Daher, N.; Shafer, M. M.; Schauer, J. J.; Sioutas, C. Global Perspective on the Oxidative Potential of Airborne Particulate Matter: A Synthesis of Research Findings. *Environ. Sci. Technol.* **2014**, *48*, 7576−7583.
(32) Tao, F.; Gonzalez-Flecha, B.; Kobzik, L. Reactive Oxygen Species in Pulmonary Inflammation by Ambient Particulates. *Free Radical Biol. Med.* **2003**, *35*, 327−340.
(33) Pöschl, U.; Shiraiwa, M. Multiphase Chemistry at the Atmosphere−Biosphere Interface Influencing Climate and Public Health in the Anthropocene. *Chem. Rev.* **2015**, *115*, 4440−4475.
(34) Mills, I. C.; Atkinson, R. W.; Kang, S.; Walton, H.; Anderson, H. R. Quantitative Systematic Review of the Associations between Short-Term Exposure to Nitrogen Dioxide and Mortality and Hospital Admissions. *BMJ Open* **2015**, *5*, No. e006946.
(35) Faustini, A.; Rapp, R.; Forastiere, F. Nitrogen Dioxide and Mortality: Review and Meta-Analysis of Long-Term Studies. *Eur. Respir. J.* **2014**, *44*, 744−753.
(36) European WHO Regional Office. Review of Evidence on Health Aspects of Air Pollution−REVIHAAP Project: Technical Report, 2013.
(37) Burnett, R. T.; Stieb, D.; Brook, J. R.; Cakmak, S.; Dales, R.; Raizenne, M.; Vincent, R.; Dann, T. Associations between Short-Term Changes in Nitrogen Dioxide and Mortality in Canadian Cities. *Arch. Environ. Health* **2004**, *59*, 228−236.
(38) Postlethwait, E.; Bidani, A. Mechanisms of Pulmonary NO2 Absorption. *Toxicology* **1994**, *89*, 217−237.
(39) Lancaster, J. R. Nitroxidative, Nitrosative, and Nitrative Stress: Kinetic Predictions of Reactive Nitrogen Species Chemistry Under Biological Conditions. *Chem. Res. Toxicol.* **2006**, *19*, 1160−1174.
(40) Kirsch, M.; Lehnig, M.; Korth, H.-G.; Sustmann, R.; de Groot, H. Inhibition of Peroxynitrite-Induced Nitration of Tyrosine by Glutathione in the Presence of Carbon Dioxide through Both Radical Repair and Peroxynitrate Formation. *Chem. − Eur. J.* **2001**, *7*, 3313−3320.
(41) McConnell, R.; Berhane, K.; Gilliland, F.; London, S. J.; Islam, T.; Gauderman, W. J.; Avol, E.; Margolis, H. G.; Peters, J. M. Asthma in Exercising Children Exposed to Ozone: A Cohort Study. *Lancet* **2002**, *359*, 386−391.
(42) Mudway, I. S.; Kelly, F. J. Ozone and the Lung: A Sensitive Issue. *Mol. Aspects Med.* **2000**, *21*, 1−48.
(43) Hewitt, C. N.; Kok, G. L. Formation and Occurrence of Organic Hydroperoxides in the Troposphere: Laboratory and Field Observations. *J. Atmos. Chem.* **1991**, *12*, 181−194.
(44) Hasson, A. S.; Ho, A. W.; Kuwata, K. T.; Paulson, S. E. Production of Stabilized Criegee Intermediates and Peroxides in the Gas Phase Ozonolysis of Alkenes: 2. Asymmetric and Biogenic Alkenes. *J. Geophys. Res.* **2001**, *106*, 34143−34153.
(45) Long, N. C.; Suh, J.; Morrow, J. D.; Schiestl, R. H.; Murthy, G. G. K.; Brain, J. D.; Frei, B. Ozone Causes Lipid Peroxidation but Little Antioxidant Depletion in Exercising and Nonexercising Hamsters. *J. Appl. Physiol.* **2001**, *91*, 1694−1700.
(46) Sies, H. Strategies of Antioxidant Defense. *Eur. J. Biochem.* **1993**, *215*, 213−219.
(47) Cantin, A. M.; Fells, G. A.; Hubbard, R. C.; Crystal, R. G. Antioxidant Macromolecules in the Epithelial Lining Fluid of the Normal Human Lower Respiratory Tract. *J. Clin. Invest.* **1990**, *86*, 962−971.
(48) Johnson, F.; Giulivi, C. Superoxide Dismutases and Their Impact upon Human Health. *Mol. Aspects Med.* **2005**, *26*, 340−352.
(49) Forman, H. J.; Davies, K. J. A.; Ursini, F. How Do Nutritional Antioxidants Really Work: Nucleophilic Tone and Para-Hormesis versus Free Radical Scavenging in Vivo. *Free Radical Biol. Med.* **2014**, *66*, 24−35.
(50) Ray, P. D.; Huang, B.-W.; Tsuji, Y. Reactive Oxygen Species (ROS) Homeostasis and Redox Regulation in Cellular Signaling. *Cell. Signal.* **2012**, *24*, 981−990.
(51) Dröge, W. Free Radicals in the Physiological Control of Cell Function. *Physiol. Rev.* **2002**, *82*, 47−95.
(52) Zhang, Z.; Weichenthal, S.; Kwong, J. C.; Burnett, R. T.; Hatzopoulou, M.; Jerrett, M.; et al. A Population-Based Cohort Study of Respiratory Disease and Long-Term Exposure to Iron and Copper in Fine Particulate Air Pollution and Their Combined Impact on Reactive Oxygen Species Generation in Human Lungs. *Environ. Sci. Technol.* **2021**, *55*, 3807−3818.
(53) Weichenthal, S.; Shekarrizfard, M.; Kulka, R.; Lakey, P. S. J.; Al-Rijleh, K.; Anowar, S.; Shiraiwa, M.; Hatzopoulou, M. Spatial Variations in the Estimated Production of Reactive Oxygen Species in the Epithelial Lung Lining Fluid by Iron and Copper in Fine Particulate Air Pollution. *Environ. Epidemiol.* **2018**, *2*, No. e020.
(54) Zhang, Z.; Weichenthal, S.; Kwong, J. C.; Burnett, R. T.; Hatzopoulou, M.; Jerrett, M.; van Donkelaar, A.; Bai, L.; Martin, R. V.; Copes, R.; Lu, H.; Lakey, P.; Shiraiwa, M.; Chen, H. Long-Term Exposure to Iron and Copper in Fine Particulate Air Pollution and Their Combined Impact on Reactive Oxygen Species Concentration in Lung Fluid: A Population-Based Cohort Study of Cardiovascular Disease Incidence and Mortality in Toronto, Canada. *Int. J. Epidemiol.* **2021**, *50*, 589−601.
(55) Stieb, D. M.; Evans, G. J.; To, T. M.; Lakey, P. S. J.; Shiraiwa, M.; Hatzopoulou, M.; Minet, L.; Brook, J. R.; Burnett, R. T.; Weichenthal, S. A. Within-City Variation in Reactive Oxygen Species from Fine Particle Air Pollution and COVID-19. *Am. J. Respir. Crit. Care Med.* **2021**, *204*, 168−177, DOI: 10.1164/rccm.202011-4142OC.
(56) Pizzino, G.; Irrera, N.; Cucinotta, M.; Pallio, G.; Mannino, F.; Arcoraci, V.; Squadrito, F.; Altavilla, D.; Bitto, A. Oxidative Stress: Harms and Benefits for Human Health. *Oxid. Med. Cell. Longevity* **2017**, *2017*, No. 8416763.
(57) Young, I. S. Antioxidants in Health and Disease. *J. Clin. Pathol.* **2001**, *54*, 176−186.
(58) Walling, C. Fenton's Reagent Revisited. *Acc. Chem. Res.* **1975**, *8*, 125−131.

(59) Vidrio, E.; Phuah, C.; Dillner, A. M.; Anastasio, C. Generation of Hydroxyl Radicals from Ambient Fine Particles in a Surrogate Lung Fluid Solution. *Environ. Sci. Technol.* **2009**, *43*, 922−927.
(60) Shiraiwa, M.; Pfrang, C.; Poschl, U. Kinetic Multi-Layer Model of Aerosol Surface and Bulk Chemistry (KM-SUB): The Influence of Interfacial Transport and Bulk Diffusion on the Oxidation of Oleic Acid by Ozone. *Atmos. Chem. Phys.* **2010**, *10*, 3673−3691.
(61) Saunders, S. M.; Jenkin, M. E.; Derwent, R. G.; Pilling, M. J. Protocol for the Development of the Master Chemical Mechanism, MCM v3 (Part A): Tropospheric Degradation of Non-Aromatic Volatile Organic Compounds. *Atmos. Chem. Phys.* **2003**, *3*, 161−180.
(62) Jenkin, M. E.; Saunders, S. M.; Wagner, V.; Pilling, M. J. Protocol for the Development of the Master Chemical Mechanism, MCM v3 (Part B): Tropospheric Degradation of Aromatic Volatile Organic Compounds. *Atmos. Chem. Phys.* **2003**, *3*, 181−193.
(63) Wang, Y.; Kim, H.; Paulson, S. E. Hydrogen Peroxide Generation from α- and β-Pinene and Toluene Secondary Organic Aerosols. *Atmos. Environ.* **2011**, *45*, 3149−3156.
(64) Sarangapani, R. The Role of Dispersion in Particle Deposition in Human Airways. *Toxicol. Sci.* **2000**, *54*, 229−236.
(65) Shi, X.; Brasseur, G. P. The Response in Air Quality to the Reduction of Chinese Economic Activities during the COVID-19 Outbreak. *Geophys. Res. Lett.* **2020**, *47*, 1−8.
(66) Andreae, M. O.; Acevedo, O. C.; Araùjo, A.; Artaxo, P.; Barbosa, C. G. G.; Barbosa, H. M. J.; Brito, J.; Carbone, S.; Chi, X.; Cintra, B. B. L.; da Silva, N. F.; Dias, N. L.; Dias-Júnior, C. Q.; Ditas, F.; Ditz, R.; Godoi, A. F. L.; Godoi, R. H. M.; Heimann, M.; Hoffmann, T.; Kesselmeier, J.; Könemann, T.; Krüger, M. L.; Lavric, J. V.; Manzi, A. O.; Lopes, A. P.; Martins, D. L.; Mikhailov, E. F.; Moran-Zuloaga, D.; Nelson, B. W.; Nölscher, A. C.; Santos Nogueira, D.; Piedade, M. T. F.; Pöhlker, C.; Pöschl, U.; Quesada, C. A.; Rizzo, L. V.; Ro, C.-U.; Ruckteschler, N.; Sá, L. D. A.; de Oliveira Sá, M.; Sales, C. B.; dos Santos, R. M. N.; Saturno, J.; Schöngart, J.; Sörgel, M.; de Souza, C. M.; de Souza, R. A. F.; Su, H.; Targhetta, N.; Tóta, J.; Trebs, I.; Trumbore, S.; van Eijck, A.; Walter, D.; Wang, Z.; Weber, B.; Williams, J.; Winderlich, J.; Wittmann, F.; Wolff, S.; Yáñez-Serrano, A. M. The Amazon Tall Tower Observatory (ATTO): Overview of Pilot Measurements on Ecosystem Ecology, Meteorology, Trace Gases, and Aerosols. *Atmos. Chem. Phys.* **2015**, *15*, 10723−10776.
(67) Fleming, Z. L.; Doherty, R. M.; von Schneidemesser, E.; Malley, C. S.; Cooper, O. R.; Pinto, J. P.; Colette, A.; Xu, X.; Simpson, D.; Schultz, M. G.; Lefohn, A. S.; Hamad, S.; Moolla, R.; Solberg, S.; Feng, Z. Tropospheric Ozone Assessment Report: Present-Day Ozone Distribution and Trends Relevant to Human Health. *Elementa* **2018**, *6*, 12.
(68) Corradi, M.; Pignatti, P.; Brunetti, G.; Goldoni, M.; Nava, S.; Moscato, G.; Balbi, B. Comparison between Exhaled and Bronchoalveolar Lavage Levels of Hydrogen Peroxide in Patients with Diffuse Interstitial Lung Diseases. *Acta Biomed.* **2008**, *79*, 73−78.
(69) Kietzmann, D.; Kahl, R.; Müller, M.; Burchardi, H.; Kettler, D. Hydrogen Peroxide in Expired Breath Condensate of Patients with Acute Respiratory Failure and with ARDS. *Intensive Care Med.* **1993**, *19*, 78−81.
(70) Kelly, F. J.; Blomberg, A.; Frew, A.; Holgate, S. T.; Sandstrom, T. Antioxidant Kinetics in Lung Lavage Fluid Following Exposure of Humans to Nitrogen Dioxide. *Am. J. Respir. Crit. Care Med.* **1996**, *154*, 1700−1705.
(71) Gonzalez, D. H.; Diaz, D. A.; Baumann, J. P.; Ghio, A. J.; Paulson, S. E. Effects of Albumin, Transferrin and Humic-like Substances on Iron-Mediated OH Radical Formation in Human Lung Fluids. *Free Radical Biol. Med.* **2021**, *165*, 79−87.
(72) Zhou, Z.; Abbatt, J. P. D. Formation of Gas-Phase Hydrogen Peroxide via Multiphase Ozonolysis of Unsaturated Lipids. *Environ. Sci. Technol. Lett.* **2021**, *8*, 114−120.
(73) Gutteridge, J. M. Lipid Peroxidation and Antioxidants as Biomarkers of Tissue Damage. *Clin. Chem.* **1995**, *41*, 1819−1828.
(74) Pryor, W. A. Oxy-Radicals and Related Species: Their Formation, Lifetimes, and Reactions. *Annu. Rev. Physiol.* **1986**, *48*, 657−667.
(75) McCord, J. M. The Evolution of Free Radicals and Oxidative Stress. *Am. J. Med.* **2000**, *108*, 652−659.
(76) Heller, M. I.; Croot, P. L. Kinetics of Superoxide Reactions with Dissolved Organic Matter in Tropical Atlantic Surface Waters near Cape Verde (TENATSO). *J. Geophys. Res.* **2010**, *115*, No. C12038.
(77) Hayyan, M.; Hashim, M. A.; AlNashef, I. M. Superoxide Ion: Generation and Chemical Implications. *Chem. Rev.* **2016**, *116*, 3029−3085.
(78) Wei, J.; Fang, T.; Wong, C.; Lakey, P. S. J.; Nizkorodov, S. A.; Shiraiwa, M. Superoxide Formation from Aqueous Reactions of Biogenic Secondary Organic Aerosols. *Environ. Sci. Technol.* **2021**, *55*, 260−270.
(79) Sies, H. Hydrogen Peroxide as a Central Redox Signaling Molecule in Physiological Oxidative Stress: Oxidative Eustress. *Redox Biol.* **2017**, *11*, 613−619.
(80) Winterbourn, C. C. Reconciling the Chemistry and Biology of Reactive Oxygen Species. *Nat. Chem. Biol.* **2008**, *4*, 278−286.
(81) Sies, H. Oxidative Stress: Oxidants and Antioxidants. *Exp. Physiol.* **1997**, *82*, 291−295.
(82) World Health Organization. World Health Organization. Air Quality Guidelines: Global Update 2005: Particulate Matter, Ozone, Nitrogen Dioxide, and Sulfur Dioxide, 2006.
(83) Hunt, J. F.; Fang, K.; Malik, R.; Snyder, A.; Malhotra, N.; Platts-Mills, T. A. E.; Gaston, B. Endogenous Airway Acidification: Implications for Asthma Pathophysiology. *Am. J. Respir. Crit. Care Med.* **2000**, *161*, 694−699.
(84) Tate, S.; MacGregor, G.; Davis, M.; Innes, J.; Greening, A. Airways in Cystic Fibrosis Are Acidified: Detection by Exhaled Breath Condensate. *Thorax* **2002**, *57*, 926−929.
(85) Fang, T.; Guo, H.; Zeng, L.; Verma, V.; Nenes, A.; Weber, R. J. Highly Acidic Ambient Particles, Soluble Metals, and Oxidative Potential: A Link between Sulfate and Aerosol Toxicity. *Environ. Sci. Technol.* **2017**, *51*, 2611−2620.
(86) Jones, P.; Suggett, A. The Catalase−Hydrogen Peroxide System. Kinetics of Catalatic Action at High Substrate Concentrations. *Biochem. J.* **1968**, *110*, 617−620.
(87) Qiu, J.; Tonokura, K.; Enami, S. Proton-Catalyzed Decomposition of α-Hydroxyalkyl-Hydroperoxides in Water. *Environ. Sci. Technol.* **2020**, *54*, 10561−10569.
(88) Koppenol, W. H.; Hider, R. H. Iron and Redox Cycling. Do's and Don'ts. *Free Radical Biol. Med.* **2019**, *133*, 3−10.
(89) Bataineh, H.; Pestovsky, O.; Bakac, A. PH-Induced Mechanistic Changeover from Hydroxyl Radicals to Iron(Iv) in the Fenton Reaction. *Chem. Sci.* **2012**, *3*, 1594.
(90) Hug, S. J.; Leupin, O. Iron-Catalyzed Oxidation of Arsenic(III) by Oxygen and by Hydrogen Peroxide: PH-Dependent Formation of Oxidants in the Fenton Reaction. *Environ. Sci. Technol.* **2003**, *37*, 2734−2742.

https://doi.org/10.1021/acs.est.1c03875
Environ. Sci. Technol. 2021, 55, 14069−14079